A. Parrinello, G.L. Ghiringhelli, N. Atalla
Generalized Transfer Matrix Method for Periodic Planar Media
Journal of Sound and Vibration, Vol. 464, 2020, p. 1-13
doi:10.1016/j.jsv.2019.114993

Generalized Transfer Matrix Method for Periodic Planar Media

A. Parrinello[a,*], G. L. Ghiringhelli[b], N. Atalla[a]

[a] *Université de Sherbrooke 2500, Boulevard de l'Université Sherbrooke (Québec) J1K 2R1*
[b] *Politecnico di Milano,Via La Masa 34, 20156 Milano, Italy*

Abstract

Sound transmission through infinite planar multilayered structures characterized by in-plane periodicity is accurately and efficiently predicted by exploiting free wave propagation and Bloch modes. A through-thickness transfer matrix is derived for each layer by manipulating the dynamic stiffness matrix related to a finite element model of a unit cell. The transfer matrices of all the layers composing the structure account for the Bloch modes generated in heterogeneous layers. The proposed technique is equally appealing for in-plane homogeneous structures since few elements and no Bloch modes are needed in this case, ensuring high efficiency. In such a framework, the acoustic radiation or transmission of multilayered systems excited by a plane wave can be assessed. The proposed approach is validated in case of structures consisting of heterogeneous layers by comparison with alternative approaches.

Keywords: Transfer Matrix Method, Periodic Structures, Bloch Modes

1. Introduction

Most of the models proposed in the last decades to face the problem of sound propagation in complex structures involve the characterization of the wave propagation using a wave and finite element method (WFEM). The WFEM combines conventional Finite Element (FE) models and the theory of wave propagation in

*Corresponding author
Email address: andrea.parrinello@usherbrooke.ca (A. Parrinello)

periodic structures. The mathematics of wave propagation in periodic systems has been discussed by Brillouin [1] in the field of electrical engineering. Mead [2] and Abrahamson [3] have involved the Rayleigh-Ritz technique in order to treat non-uniform periodic structures. Afterwards, Orris and Petyt [4, 5] have employed the FE technique for wave propagation analysis.

An alternative approach to model the sound propagation in complex structures is the Transfer Matrix Method [6] (TMM). Matrix representation of sound propagation is an efficient and largely used tool for modeling plane acoustic fields in stratified media. The problem is formulated in the frequency domain and layers are assumed to be laterally infinite. In the classical TMM, all the waves propagating within each layer of the structure are assumed to have the same in-plane wavenumber components of the plane wave excitation coming from a bounding semi-infinite fluid. Analytical expressions for the Transfer Matrices (TMs) are only available for homogeneous media [6]. The TM of a periodic layer is obtained in [7] by manipulating the Dynamic Stiffness Matrix (DSM) of a layer's periodic Unit Cell (UC). However, because of the aforementioned assumption regarding the in-plane wavenumber components, the approach proposed in [7] fails to fully capture the physics of sound propagation in periodic structures when the in-plane dimensions of the UCs are similar or greater than the excitation wavelength. In fact, within a heterogeneous layer, a plane wave excitation can produce different waves because of the periodicity. These additional waves are the Bloch modes and can propagate within the structure, thus contributing to the sound propagation. This paper proposes a generalization of the TM approach proposed in [7]. Bloch modes are considered in heterogeneous layers and their propagation is modeled within each layer composing the structure, including the homogeneous layers. As a consequence, the dimensions of the resulting TMs depend on the number of Bloch modes considered.

The paper is composed of two parts. First, the theory on the basis of the proposed approach is derived. The plane wave excitation and the coupling with the semi-infinite fluid media are modeled, the TMs of both homogeneous and heterogeneous layers are derived, the global system is assembled and the acoustic

indicators are evaluated. Then, the proposed approach is validated in case of structures consisting of heterogeneous layers by comparison with alternative approaches. Results are presented in the case of an oblique plane wave acting on the bottom surface of the multilayered structures for both semi-infinite fluid and hard-wall terminations.

2. Theory

Let us consider a multilayered structure with infinite lateral extent surrounded by two semi-infinite non-dispersive media, *i.e.* ideal fluids, or backed by a hard wall. The structure lies on the xy-plane and the sound propagation through its thickness (z-axis) is studied. Subscripts B and T indicating values at the bottom and top surfaces of the structure or properties of the lower and upper fluids. The fluids have thus densities and wave speeds $\rho_{B,T}$ and $c_{B,T}$ respectively. Throughout the analysis we assume time-harmonic motion of the form $\exp(\mathrm{j}\omega t)$.

2.1. Acoustic Excitation

The structure is excited by a plane wave traveling in the lower fluid and impinging its bottom surface with an incident angle, θ, with respect to the z-axis and a heading angle, ϕ, with respect to the x-axis. The incident pressure field can be expressed as

$$P_I = p_0 e^{\mathrm{j}(\omega t - k_x x - k_y y - k_z z)}, \tag{1}$$

where p_0 is the wave amplitude and the wavenumber components are

$$\begin{cases} k_x = \dfrac{\omega}{c_B} \sin\theta \cos\phi \\ k_y = \dfrac{\omega}{c_B} \sin\theta \sin\phi \\ k_z = \dfrac{\omega}{c_B} \cos\theta \end{cases} . \tag{2}$$

The *blocked-wall* pressure (*i.e.* the real excitation seen by the structure) is obtained by assuming a Neumann boundary at the *blocked* bottom surface, thus

obtaining the total pressure field produced by the incident plane wave at the bottom surface:

$$P_b = 2p_0 e^{\mathrm{j}(\omega t - k_x x - k_y y)} = p_b e^{\mathrm{j}(\omega t - k_x x - k_y y)}. \tag{3}$$

2.2. Transfer Matrix of a Layer

In order to simplify the following exposure, only layers defined by a single physics (solid, fluid or porous) are considered. Details on the mixed formulation can be found in [7]. Anyway, different phases of the same nature are allowed within a layer. Porous media can also be represented as equivalent fluids [6, 8, 9]. The periodic UC of a layer is represented by a right cuboid modeled using FEs and the related dynamic problem can be written as

$$\mathbf{D}(\omega)\mathbf{q} = \mathbf{f} + \mathbf{e}\ , \tag{4}$$

where $\mathbf{D}(\omega)$ is the DSM of the UC, $\mathbf{q}$ is the vector of generalized displacements or pressures, $\mathbf{f}$ is the vector of generalized internal forces, *i.e.* due to adjacent UCs, and $\mathbf{e}$ is the vector of generalized external forces, *i.e.* due to bounding media. In the following, degrees of freedom (dofs) related to a node are supposed consecutive in vector $\mathbf{q}$. On the other hand, TMs are built to have Bloch coefficients for a single dof arranged consecutively.

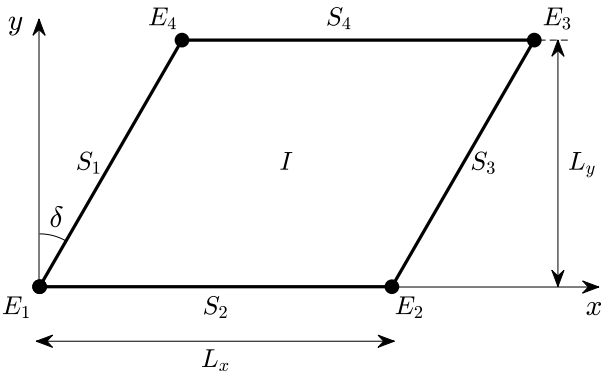

Figure 1: Partitioning of a UC into an internal region (I), surfaces S_{1-4} and edges E_{1-4}.

Homogeneous layers and heterogeneous layers are treated differently. Let us start with heterogeneous layers. Figure 1 depicts the UC of a heterogeneous

layer. In order to apply periodic boundary conditions, the UC is partitioned in an internal region (I), four surfaces (S_{1-4}) and four edges (E_{1-4}). It should be noted that all the heterogeneous layers of the structure must have the same in-plane dimensions (L_x,L_y) and shape (δ) in order to grant compatibility between all the Bloch modes throughout the whole structure. Bloch's theorem must be applied to the generalized displacements vector as

$$\mathbf{q} = \left(\mathbf{\Lambda}_0 + \mathbf{\Lambda}_x e^{\mathrm{j}k_x L_x} + \mathbf{\Lambda}_y e^{\mathrm{j}\tilde{k}_y L_y} + \mathbf{\Lambda}_{xy} e^{\mathrm{j}(k_x L_x + \tilde{k}_y L_y)}\right) \mathbf{q}' = \mathbf{A}\mathbf{q}' \ , \tag{5}$$

where $\mathbf{\Lambda}_X$ are linear interpolation matrices linking nodal displacements and pressures at the slave boundaries (S_{3-4}, E_{2-4}) to the nodal values at the master boundaries (S_{1-2}, E_1), $\tilde{k}_y = k_y + k_x \tan\delta$ and the wavenumber components, k_x and k_y, are defined in Eq. (2). Interpolation matrices allow to handle UCs with different meshes at opposite boundaries, making the procedure less restrictive in terms of mesh requirements. Thus, the equation of motion, Eq. (4), can be reduced as

$$\mathbf{A}^H \mathbf{D}(\omega)\mathbf{A}\mathbf{q}' = \mathbf{D}'(\omega, k_x, k_y)\mathbf{q}' = \mathbf{A}^H(\mathbf{f} + \mathbf{e}) \ . \tag{6}$$

Under the assumption of real wavenumbers, the forces due to neighboring cells disappear from the dynamic problem [7] and the equation of motion becomes

$$\mathbf{D}'(\omega, k_x, k_y)\mathbf{q}' = \mathbf{e}' \ . \tag{7}$$

In order to evaluate the TM of the heterogeneous layer, the problem must be partitioned in top (T), bottom (B) and internal (I) sets along the thickness. Since no internal forces are applied, the set of internal dofs, $\mathbf{q}'_I$, can be removed and the problem can be arranged as

$$\begin{bmatrix} \mathbf{D}'_{BB} - \mathbf{D}'_{BI}\mathbf{D}'^{-1}_{II}\mathbf{D}'_{IB} & \mathbf{D}'_{BT} - \mathbf{D}'_{BI}\mathbf{D}'^{-1}_{II}\mathbf{D}'_{IT} \\ \mathbf{D}'_{TB} - \mathbf{D}'_{TI}\mathbf{D}'^{-1}_{II}\mathbf{D}'_{IB} & \mathbf{D}'_{TT} - \mathbf{D}'_{TI}\mathbf{D}'^{-1}_{II}\mathbf{D}'_{IT} \end{bmatrix} \begin{Bmatrix} \mathbf{q}'_B \\ \mathbf{q}'_T \end{Bmatrix} = \mathbf{C}' \begin{Bmatrix} \mathbf{q}'_B \\ \mathbf{q}'_T \end{Bmatrix} = \begin{Bmatrix} \mathbf{e}'_B \\ \mathbf{e}'_T \end{Bmatrix} . \tag{8}$$

To build the corresponding one dimensional model, we first define the matrices

$$\begin{aligned} \mathbf{L}_B &= \begin{bmatrix} \mathbf{A}_B \otimes \mathbf{I}_{m,1} & \dots & \mathbf{A}_B \otimes \mathbf{I}_{m,m} \end{bmatrix} \\ \mathbf{L}_T &= \begin{bmatrix} \mathbf{A}_T \otimes \mathbf{I}_{m,1} & \dots & \mathbf{A}_T \otimes \mathbf{I}_{m,m} \end{bmatrix} \end{aligned} \tag{9}$$

where $\mathbf{I}_{m,i}$ is the i-th column of the identity matrix of size m, m is the number of dofs for each node (1 for fluid layers, 3 for solid layers, 4 for porous layers), $\otimes$ denotes the Kronecker product, matrices $\mathbf{A}_B$ and $\mathbf{A}_T$ are defined as

$$\mathbf{A}_B = \exp\left(\mathrm{j}\mathbf{x}_B\mathcal{X} + \mathrm{j}\mathbf{y}_B\Upsilon\right) \ , \ \mathbf{A}_T = \exp\left(\mathrm{j}\mathbf{x}_T\mathcal{X} + \mathrm{j}\mathbf{y}_T\Upsilon\right) \ , \tag{10}$$

$\mathbf{x}|\mathbf{y}_{B|T}$ are column vectors collecting nodal coordinates, $\mathcal{X}$ and Υ are row vectors collecting the wavenumber components of the Bloch modes as

$$\mathcal{X} = k_x + \frac{2\pi}{L_x}\mathbf{n}_x \ , \ \Upsilon = k_y + \frac{2\pi}{L_y}\mathbf{n}_y - \frac{2\pi}{L_x}\mathbf{n}_x \tan\delta \ , \tag{11}$$

$\mathbf{n}_x$ and $\mathbf{n}_y$ are row vectors defined as

$$\mathbf{n}_x = \mathbf{O}_{2N_y+1} \otimes \begin{bmatrix} -N_x & \dots & N_x \end{bmatrix} \ , \ \mathbf{n}_y = \begin{bmatrix} -N_y & \dots & N_y \end{bmatrix} \otimes \mathbf{O}_{2N_x+1} \ , \tag{12}$$

N_x and N_y are the maximum orders of Bloch modes selected and $\mathbf{O}_n$ is a row vector of ones of size n. It should be noted that the M-th column of matrices $\mathbf{A}_B$ and $\mathbf{A}_T$ represents the exciting plane wave ($n_x = n_y = 0$), with $M = 2N_xN_y + N_x + N_y + 1$. Thus, the through-thickness one dimensional dynamic problem can be derived as

$$\begin{bmatrix} \mathbf{L}_B^H\mathbf{C}'_{BB}\mathbf{L}_B & \mathbf{L}_B^H\mathbf{C}'_{BT}\mathbf{L}_T \\ \mathbf{L}_T^H\mathbf{C}'_{TB}\mathbf{L}_B & \mathbf{L}_T^H\mathbf{C}'_{TT}\mathbf{L}_T \end{bmatrix} \begin{Bmatrix} \hat{\mathbf{q}}_B \\ \hat{\mathbf{q}}_T \end{Bmatrix} = \mathbf{C} \begin{Bmatrix} \hat{\mathbf{q}}_B \\ \hat{\mathbf{q}}_T \end{Bmatrix} = \begin{Bmatrix} \hat{\mathbf{e}}_B \\ \hat{\mathbf{e}}_T \end{Bmatrix} \ . \tag{13}$$

Finally, the problem can be rearranged in terms of a transfer matrix as

$$\begin{bmatrix} -\mathbf{C}_{TB}^{-1}\mathbf{C}_{TT} & \mathbf{C}_{TB}^{-1} \\ \mathbf{C}_{BT} - \mathbf{C}_{BB}\mathbf{C}_{TB}^{-1}\mathbf{C}_{TT} & \mathbf{C}_{BB}\mathbf{C}_{TB}^{-1} \end{bmatrix} \begin{Bmatrix} \hat{\mathbf{q}}_T \\ \hat{\mathbf{e}}_T \end{Bmatrix} = \mathbf{T}'(\omega, k_x, k_y) \begin{Bmatrix} \hat{\mathbf{q}}_T \\ \hat{\mathbf{e}}_T \end{Bmatrix} = \begin{Bmatrix} \hat{\mathbf{q}}_B \\ \hat{\mathbf{e}}_B \end{Bmatrix} \ . \tag{14}$$

The TM, $\mathbf{T}'$, of a heterogeneous layer is a $2Nm \times 2Nm$ full populated matrix where $N = (2N_x + 1)(2N_y + 1)$ is the number of Bloch modes.

The TM, $\mathbf{T}'$, of a homogeneous layer must now be evaluated. Since waves with different wavenumbers propagate independently within homogeneous media, the TM of a homogeneous layer is a $2Nm \times 2Nm$ sparse matrix composed of elementary TMs. For the selected ordering rule, the elementary TM related to the i-th Bloch mode, $\mathbf{T}'_i$, is the sub-matrix of $\mathbf{T}'$ with row indices and column indices equal to the vector $[N(\mathbf{r} - 1) + i]$ where vector $\mathbf{r}$ spans from 1 to $2m$.

In order to achieve the higher possible efficiency and to simplify the following exposure, homogeneous layers are modeled with cubical UCs having nodes located only at the vertices. The discretization along the thickness of the layer is handled within the TM context. The edge of the UC, l, is selected as a fraction of the layer thickness, h, ($l = h/n_z$) and the layer TM is obtained as power of the UC TM ($\mathbf{T}_{\text{layer}} = \mathbf{T}_{\text{UC}}^{n_z}$). In order to obtain the i-th TM of the layer, $\mathbf{T}'_i$, the generalized displacements vector must be reduced according to the i-th Bloch mode as

$$\mathbf{q} = \left(\mathbf{\Lambda}_0 + \mathbf{\Lambda}_x e^{\mathrm{j}\mathcal{X}_i l} + \mathbf{\Lambda}_y e^{\mathrm{j}\Upsilon_i l} + \mathbf{\Lambda}_{xy} e^{\mathrm{j}(\mathcal{X}_i l + \Upsilon_i l)}\right) \mathbf{q}' = \mathbf{A}_i \mathbf{q}' \ , \tag{15}$$

where $\mathcal{X}_i$ and Υ_i are the i-th elements of vectors $\mathcal{X}$ and Υ. Because of the simplified UC model, we obtain directly

$$\mathbf{C}(\omega, \mathcal{X}_i, \Upsilon_i) = \mathbf{A}_i^H \mathbf{D}(\omega) \mathbf{A}_i \tag{16}$$

and

$$\mathbf{T}'_i(\omega, \mathcal{X}_i, \Upsilon_i) = \begin{bmatrix} -\mathbf{C}_{TB}^{-1}\mathbf{C}_{TT} & \mathbf{C}_{TB}^{-1} \\ \mathbf{C}_{BT} - \mathbf{C}_{BB}\mathbf{C}_{TB}^{-1}\mathbf{C}_{TT} & \mathbf{C}_{BB}\mathbf{C}_{TB}^{-1} \end{bmatrix} \ . \tag{17}$$

2.3. Modifying Interface Variables

The TM, $\mathbf{T}'$, is now modified in order to simplify the inter-layer boundary conditions. For each Bloch mode, new state vectors, $\mathbf{V}_T$ and $\mathbf{V}_B$, are related to the original state vectors, $\mathbf{V}'_T = [\hat{\mathbf{q}}_T \ \ \hat{\mathbf{e}}_T]^T$ and $\mathbf{V}'_B = [\hat{\mathbf{q}}_B \ \ \hat{\mathbf{e}}_B]^T$ as

$$\mathbf{V}'_T = \mathbf{\Lambda}_T \mathbf{V}_T \ , \ \mathbf{V}_B = \mathbf{\Lambda}_B \mathbf{V}'_B \ , \tag{18}$$

thus obtaining the final form of the TM of a heterogeneous layer as

$$\mathbf{T} = \left((\mathbf{\Lambda}_B \otimes \mathbf{I}_N)\mathbf{T}'(\mathbf{\Lambda}_T \otimes \mathbf{I}_N)\right)^{n_z} \ , \tag{19}$$

where $\mathbf{I}_N$ is the identity matrix of size N and n_z is the ratio between the layer thickness and the UC thickness, and the i-th TM of a homogneous layer as

$$\mathbf{T}_i = \left(\mathbf{\Lambda}_B \mathbf{T}'_i \mathbf{\Lambda}_T\right)^{n_z} \ . \tag{20}$$

The original and the chosen state vectors for a fluid layer are respectively

$$\mathbf{V}'_f = \begin{bmatrix} p & -\mathrm{j}\omega A v_n^f \end{bmatrix}^T \ , \ \mathbf{V}_f = \begin{bmatrix} p & v_z^f \end{bmatrix}^T \tag{21}$$

where v_n^f is the (outward-pointing) normal velocity and the area of the UC, A, is equal to $L_x L_y$ for heterogeneous layers or l^2 for homogeneous layers. As a consequence, the related transformation matrices are

$$\mathbf{\Lambda}_B = \mathrm{diag}\begin{bmatrix} 1 & 1/\mathrm{j}\omega A \end{bmatrix} \ , \ \mathbf{\Lambda}_T = \mathrm{diag}\begin{bmatrix} 1 & -\mathrm{j}\omega A \end{bmatrix} \ . \tag{22}$$

The state vectors for a solid layer are

$$\mathbf{V}'_s = \begin{bmatrix} u_x & u_y & u_z & F_x & F_y & F_z \end{bmatrix}^T \ , \ \mathbf{V}_s = \begin{bmatrix} v_x^s & v_y^s & v_z^s & \sigma_{zx} & \sigma_{zy} & \sigma_{zz} \end{bmatrix}^T \tag{23}$$

and the related transformation matrices are

$$\mathbf{\Lambda}_B = \mathrm{diag}\begin{bmatrix} \mathbf{O}_3 \mathrm{j}\omega & -\mathbf{O}_3/A \end{bmatrix} \ , \ \mathbf{\Lambda}_T = \mathrm{diag}\begin{bmatrix} \mathbf{O}_3/\mathrm{j}\omega & \mathbf{O}_3 A \end{bmatrix} \ . \tag{24}$$

The state vector related to the chosen porous formulation [10] is

$$\mathbf{V}'_p = \begin{bmatrix} u_x^s & u_y^s & u_z^s & p & F_x^s & F_y^s & F_z^s & -\mathrm{j}\omega A(v_n^f + v_n^s \tilde{\gamma}/\Phi^2) \end{bmatrix}^T \tag{25}$$

where Φ is the layer porosity and $\tilde{\gamma}$ is a coupling coefficient between the solid and the fluid phase of the porous media. On the other hand, the chosen state vector is

$$\mathbf{V}_p = \begin{bmatrix} v_x^s & v_y^s & v_z^s & p & \sigma_{zx}^s & \sigma_{zy}^s & \sigma_{zz}^t & w \end{bmatrix}^T \tag{26}$$

where $w = \Phi(v_z^f - v_z^s)$ is the flux per unit area at the interface, $\sigma_{zz}^t = \sigma_{zz}^s + \sigma_{zz}^f$ is the total normal stress and $\sigma_{zz}^f = -p\Phi$ is the equivalent normal stress due to the fluid. The related transformation matrices are

$$\mathbf{\Lambda}_T = \left[\begin{array}{cccc|cccc} 1/\mathrm{j}\omega & 0 & 0 & 0 & 0 & 0 & 0 & 0 \\ 0 & 1/\mathrm{j}\omega & 0 & 0 & 0 & 0 & 0 & 0 \\ 0 & 0 & 1/\mathrm{j}\omega & 0 & 0 & 0 & 0 & 0 \\ 0 & 0 & 0 & 1 & 0 & 0 & 0 & 0 \\ 0 & 0 & 0 & 0 & A & 0 & 0 & 0 \\ 0 & 0 & 0 & 0 & 0 & A & 0 & 0 \\ 0 & 0 & 0 & \Phi A & 0 & 0 & A & 0 \\ 0 & 0 & -gA & 0 & 0 & 0 & 0 & -\mathrm{j}\omega A/\Phi \end{array}\right] \tag{27}$$

and

$$\mathbf{\Lambda}_B = \left[\begin{array}{cccc|cccc} \mathrm{j}\omega & 0 & 0 & 0 & 0 & 0 & 0 & 0 \\ 0 & \mathrm{j}\omega & 0 & 0 & 0 & 0 & 0 & 0 \\ 0 & 0 & \mathrm{j}\omega & 0 & 0 & 0 & 0 & 0 \\ 0 & 0 & 0 & 1 & 0 & 0 & 0 & 0 \\ 0 & 0 & 0 & 0 & -1/A & 0 & 0 & 0 \\ 0 & 0 & 0 & 0 & 0 & -1/A & 0 & 0 \\ 0 & 0 & 0 & -\Phi & 0 & 0 & -1/A & 0 \\ 0 & 0 & -g\Phi & 0 & 0 & 0 & 0 & \Phi/\mathrm{j}\omega A \end{array}\right] \tag{28}$$

where $g = \mathrm{j}\omega(1 + \tilde{\gamma}/\Phi^2)$.

2.4. Inter-Layer Boundary Conditions

This section is devoted to the continuity conditions between adjacent layers. In case of a solid-fluid interface the following conditions must be imposed

$$\mathbf{I}_{sf}\mathbf{V}_s + \mathbf{J}_{sf}\mathbf{V}_f = \left([\mathbf{0} \quad \mathbf{I}_4] \otimes \mathbf{I}_N\right)\mathbf{V}_s + \left(\begin{bmatrix} 0 & -1 \\ 0 & 0 \\ 0 & 0 \\ 1 & 0 \end{bmatrix} \otimes \mathbf{I}_N\right)\mathbf{V}_f = \mathbf{0}. \tag{29}$$

Matrices $\mathbf{I}_{sf}$ and $\mathbf{J}_{sf}$ must be interchanged for a fluid-solid interface. The state vector $\mathbf{V}_p$ defined in Eq. (26) considerably simplifies the porous-porous and the porous-fluid interfaces, making interface conditions independent from the porosity, Φ. In fact, all the components of $\mathbf{V}_p$ are equal at each side of the boundary between two porous layers with frames bonded together. On the other hand, the following boundary conditions must be set for a porous-fluid interface

$$\mathbf{I}_{pf}\mathbf{V}_p + \mathbf{J}_{pf}\mathbf{V}_f = \left([\mathbf{0} \quad \mathbf{I}_5 \quad \mathbf{I}_{5,1}] \otimes \mathbf{I}_N\right)\mathbf{V}_p + \left(\begin{bmatrix} 0 & -1 \\ -1 & 0 \\ 0 & 0 \\ 0 & 0 \\ 1 & 0 \end{bmatrix} \otimes \mathbf{I}_N\right)\mathbf{V}_f = \mathbf{0}, \tag{30}$$

where $\mathbf{I}_{5,1}$ is the first column of the identity matrix of size 5. Matrices $\mathbf{I}_{pf}$ and $\mathbf{J}_{pf}$ must be interchanged for a fluid-porous interface. In case of a porous-solid interface the following boundary conditions must be set

$$\mathbf{I}_{ps}\mathbf{V}_p + \mathbf{J}_{ps}\mathbf{V}_s = \left(\left[\begin{array}{cc} \mathbf{I}_3 & \mathbf{0} \\ \hline \mathbf{0} & \mathbf{I}_4 \end{array}\right] \otimes \mathbf{I}_N\right)\mathbf{V}_p + \left(\begin{bmatrix} -\mathbf{I}_6 \\ \mathbf{0} \end{bmatrix} \otimes \mathbf{I}_N\right)\mathbf{V}_s = \mathbf{0}. \tag{31}$$

Matrices $\mathbf{I}_{ps}$ and $\mathbf{J}_{ps}$ must be interchanged for a solid-porous interface.

If two or more adjacent layers have the same nature (including porous layers) the global TM is simply equal to the product of the TMs of the layers. Alternatively, the interface matrices $\mathbf{I}_{ij} = \mathbf{I}_{2Nm}$ and $\mathbf{J}_{ij} = -\mathbf{I}_{2Nm}$ can be used to fulfill continuity conditions, thus retaining the state variables at the i-j interface.

2.5. External Boundary Conditions

The structure if bounded by a semi-infinite fluid on its bottom surface. For the i-th Bloch mode, the spectral pressure acting on the surface due to the bottom (up-pointing) normal spectral velocity, $v_{B,i}$, is given by $p_{B,i} = -Z_{B,i} v_{B,i}$ where

$$Z_{B,i} = \frac{\omega \rho_B}{\Re|k_{B,i}| - \jmath \Im|k_{B,i}|} \tag{32}$$

and

$$k_{B,i} = \sqrt{\frac{\omega^2}{c_B^2} - \mathcal{X}_i^2 - \Upsilon_i^2}. \tag{33}$$

It should be noted that $Z_{B,M} = \rho_B c_B / \cos\theta$.

In case of a semi-infinite fluid termination and for the i-th Bloch mode, the spectral pressure acting on the top surface of the structure due to the top (up-pointing) normal spectral velocity, $v_{T,i}$, is given by $p_{T,i} = Z_{T,i} v_{T,i}$ where

$$Z_{T,i} = \frac{\omega \rho_T}{\Re|k_{T,i}| - \jmath \Im|k_{T,i}|} \tag{34}$$

and

$$k_{T,i} = \sqrt{\frac{\omega^2}{c_T^2} - \mathcal{X}_i^2 - \Upsilon_i^2}. \tag{35}$$

It should be remarked that the negative imaginary parts in Eqs. (32) and (34) ensure evanescent waves in the semi-infinite fluid media.

In case of a hard-wall termination, all the velocity components at the top surface must be set to zero. To this end, the following termination matrices are defined:

$$\mathbf{Y}_f = \begin{bmatrix} 0 & 1 \end{bmatrix} \otimes \mathbf{I}_N \ , \ \mathbf{Y}_s = \begin{bmatrix} 1 & 0 \end{bmatrix} \otimes \mathbf{I}_{3N} \ , \ \mathbf{Y}_p = \begin{bmatrix} 1 & 0 & 0 & 0 & 0 & 0 & 0 & 0 \\ 0 & 1 & 0 & 0 & 0 & 0 & 0 & 0 \\ 0 & 0 & 1 & 0 & 0 & 0 & 0 & 0 \\ 0 & 0 & 0 & 0 & 0 & 0 & 0 & 1 \end{bmatrix} \otimes \mathbf{I}_N \ . \tag{36}$$

2.6. Assembling

Stacking all the inter-layer continuity conditions we obtain

$$\mathbf{B}'''\mathbf{V}'' = \begin{bmatrix} \mathbf{I}_{f1} & \mathbf{J}_{f1}\mathbf{T}_1 & \mathbf{0} & \cdots & \mathbf{0} & \mathbf{0} \\ \mathbf{0} & \mathbf{I}_{12} & \mathbf{J}_{12}\mathbf{T}_2 & \cdots & \mathbf{0} & \mathbf{0} \\ \vdots & \vdots & \vdots & \ddots & \vdots & \vdots \\ \mathbf{0} & \mathbf{0} & \mathbf{0} & \cdots & \mathbf{I}_{(n-1)n} & \mathbf{J}_{(n-1)n}\mathbf{T}_n \end{bmatrix} \mathbf{V}'' = \mathbf{0} \ , \quad (37)$$

where matrices $\mathbf{I}_{ij}$ and $\mathbf{J}_{ij}$ depend on the nature of the i-th and j-th layers, the suffix f denotes the fluid at the excitation side and n is the number of layers. In case of a semi-infinite fluid termination, impedance conditions must be applied at the top surface as

$$\mathbf{B}''\mathbf{V}' = \left[\begin{array}{ccc} & \mathbf{B}''' & \mathbf{0} \\ \hline \mathbf{0} & \mathbf{I}_{nf} & \mathbf{J}_{nf} \\ \hline \mathbf{0} & -\mathbf{I}_N & \mathrm{diag}(\mathbf{Z}_T) \end{array}\right] \mathbf{V}' = \mathbf{0} \ . \quad (38)$$

In case of a hard-wall termination, termination conditions must be added as

$$\mathbf{B}''\mathbf{V}' = \left[\begin{array}{cc} \mathbf{B}''' & \\ \hline \mathbf{0} & \mathbf{Y}_n \end{array}\right] \mathbf{V}' = \mathbf{0} \ . \quad (39)$$

By applying impedance conditions at the excitation side we obtain

$$\mathbf{B}'\mathbf{V}' = \left[\begin{array}{ccc} \mathbf{I}_N & \mathrm{diag}(\mathbf{Z}_B) & \mathbf{0} \\ \hline & \mathbf{B}'' & \end{array}\right] \mathbf{V}' = \mathbf{0} \ . \quad (40)$$

2.7. Solution

In order to solve the problem, Eq. (40), one component of vector $\mathbf{V}'$ must be fixed. We choose to fix arbitrarily the value of the M-th pressure to 1, *i.e.* the component related to the incident plane wave. As a consequence, the M-th row of matrix $\mathbf{B}'$ must be removed because the M-th impedance condition is involved to obtain the amplitude of the incident plane wave once the corresponding velocity is determined. Thus, we obtain the new linear system $\mathbf{B}\mathbf{V}' = \mathbf{0}$ with $V'_M = 1$, which can be rearranged in a square linear system with C unknowns as

$$\begin{bmatrix} \mathbf{B}_{1:M-1} & \mathbf{B}_{M+1:C+1} \end{bmatrix} \mathbf{V} = -\mathbf{B}_M \ , \quad (41)$$

where $\mathbf{B}_i$ is the i-th column of matrix $\mathbf{B}$, $\mathbf{B}_{i:j}$ is the matrix ranging from the i-th to the j-th column of $\mathbf{B}$ and $\mathbf{V}$ is a vector of size C obtained by removing the M-th component from vector $\mathbf{V}'$. Solving the system, Eq. (41), for $\mathbf{V}$ we obtain all the Bloch components of the normal velocity at the bottom and top surfaces as $\mathbf{v}_B^f = \mathbf{V}_{N:2N-1}$ and $\mathbf{v}_T^f = \mathbf{V}_{C-N+1:C}$ respectively.

2.8. Acoustic Indicators

Once fluid velocities at boundaries are determined, all the acoustic indicators can be evaluated. The blocked pressure can be evaluated by accounting for the M-th impedance condition as

$$p_b = 1 + Z_{B,M} v_{B,M}^f \tag{42}$$

and the amplitude of the incident plane wave is $p_0 = p_b/2$. Thus, the incident acoustic power per unit area on the bottom surface of the structure is given by

$$W_I(\theta) = \frac{p_0^2 \cos\theta}{2\rho_B c_B} \ . \tag{43}$$

The sound power per unit area exchanged between the structure and the bottom (source) semi-infinite fluid can be expressed as

$$W_B(\omega, \theta, \phi) = \frac{1}{2}\Re(p_b v_{B,M}^f) - \frac{1}{2}\sum_{i=1}^{N} \Re(Z_{B,i})|v_{B,i}^f|^2 \ . \tag{44}$$

In case of a semi-infinite fluid termination, the sound power per unit area radiated by the top surface in the receiver fluid can be expressed as

$$W_T(\omega, \theta, \phi) = \frac{1}{2}\sum_{i=1}^{N} \Re(Z_{T,i})|v_{T,i}^f|^2 \ . \tag{45}$$

Thus, we obtain the power transmission coefficient $\tau = W_T/W_I$, the transmission loss $\mathrm{TL} = -10\log_{10}(\tau)$, the power absorption coefficient $\alpha = W_B/W_I$, the power reflection coefficient $R = 1-\alpha$ and the dissipation coefficient $d = 1-R-\tau$.

3. Applications

The first case concerns the sound absorption at normal incidence of a 20 mm thick foam plate with infinite cylindrical void inclusions backed by a rigid wall. Inclusions are parallel to the y-axis, have diameter of 15 mm and are 20 mm spaced along the x-axis. The foam has properties: $\Phi = 0.95$, $\sigma = 8900$ Nsm^{-4}, $\alpha_\infty = 1.42$, $\Lambda = 180$ μm, $\Lambda' = 360$ μm, $E = 224$ kPa, $\nu = 0.4$, $\mu = 17$ %, $\rho = 6.1$ kgm^{-3}. It is modeled as an equivalent fluid according to the Johnson–Champoux–Allard rigid model [6, 8, 9]. The bottom fluid has properties $c_B = 340$ ms^{-1} and $\rho_B = 1.284$ kgm^{-3}. The structure is modeled as a single layer with a Tetra4 mesh depicted in Figure 2. Figure 3 presents the comparison of the dissipation coefficient predicted by the proposed approach (GTMM) with the result produced by a double porosity analytical model [11] and also with an alternative numerical approach based on a WFEM applied to a Periodic Unit Cell of the structure (PUC) [12]. It should be noted that, contrary to the proposed approach, the alternative approach uses a UC representing the whole multilayered structures, adds fluid layers in front and back of the structure and solves directly the coupled fluid-structure problem making it much less efficient compared to the presented method. It can be observed that Bloch modes are essential to capture the physics of the problem above 17 kHz, where they produce propagating (non-evanescent) waves in the fluid. An excellent agreement is observed between all methods over the whole frequency range by using just the ± 1 Bloch modes along the x-axis in the GTMM. In order to assess the effect of the frame dynamics on the sound absorption, the foam is now modeled with a full Biot formulation [10] and the same Tetra4 mesh depicted in Figure 2. Figure 4 shows the related dissipation coefficient predicted by the proposed approach (GTMM) along with the reference solution which employs a rigid frame model for the foam [11]. It is confirmed that the solution converges for $N_x = 1$ and it can be observed that the frame dynamics significantly affects the solution, especially above 10 kHz.

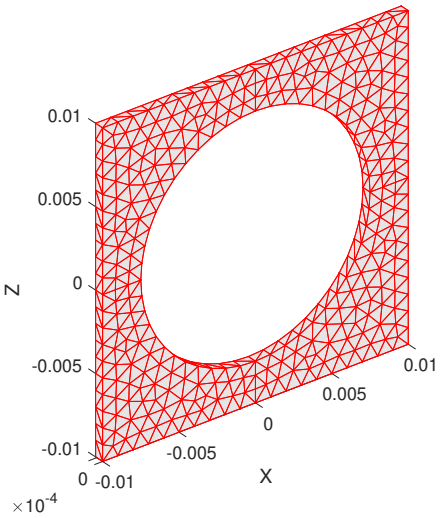

Figure 2: UC of a 20 mm thick foam plate with cylindrical inclusions.

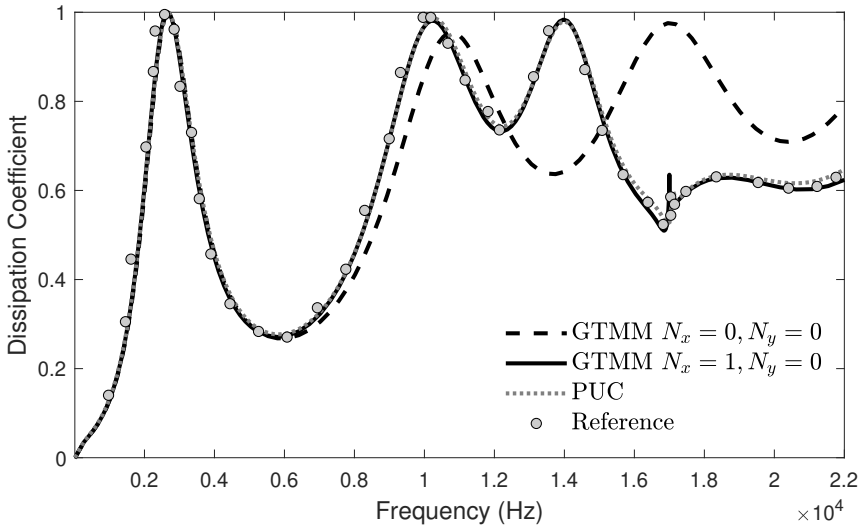

Figure 3: Dissipation coefficient at normal incidence of a 20 mm thick foam plate with cylindrical inclusions backed by a rigid wall modeled with a rigid frame model.

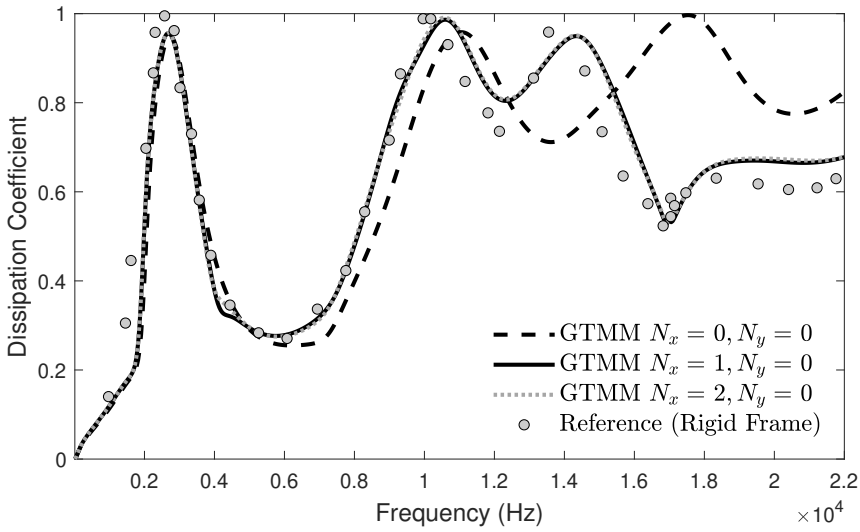

Figure 4: Dissipation coefficient at normal incidence of a 20 mm thick foam plate with cylindrical inclusions backed by a rigid wall modeled with a Biot formulation.

The second case concerns a doubly periodic coated sphere in a host rubber backed by a 15 mm thick steel plate with water on the incident side and air behind the steel plate. The core of the sphere is made of aluminum alloy while its coating is made of a soft silicon rubber. The coating has internal diameter of 10 mm and external diameter of 15 mm. The spheres are 19 mm spaced along both the x-axis and the y-axis. The host rubber is 19 mm thick. The materials properties are listed in Table 1. The fluids properties are $c_B = 1489$ ms^{-1}, $\rho_B = 1000$ kgm^{-3}, $c_T = 340$ ms^{-1}, $\rho_T = 1.29$ kgm^{-3}. The structure is modeled in two layers. Half of the Hexa27 mesh of the UC for the heterogeneous layer is depicted in Figure 5. The steel plate is modeled with one Hexa8 element and $n_z = 15$. Figure 6 compares the dissipation coefficients at two oblique incidence ($\theta = 45|75°$, $\phi = 0°$) predicted by the proposed approach (GTMM) with the result produced by an alternative numerical approach (PUC). An excellent agreement is observed between the two methods over the whole frequency range in case of few Bloch modes used in the GTMM.

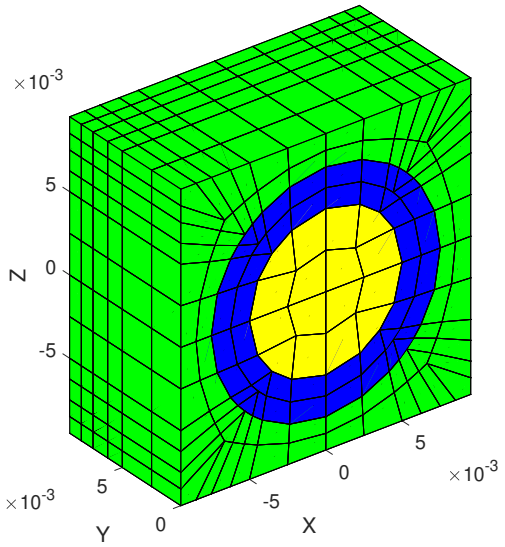

Figure 5: Half UC of a heterogeneous layer made of aluminum alloy (yellow), silicon rubber (blue) and host rubber (Green).

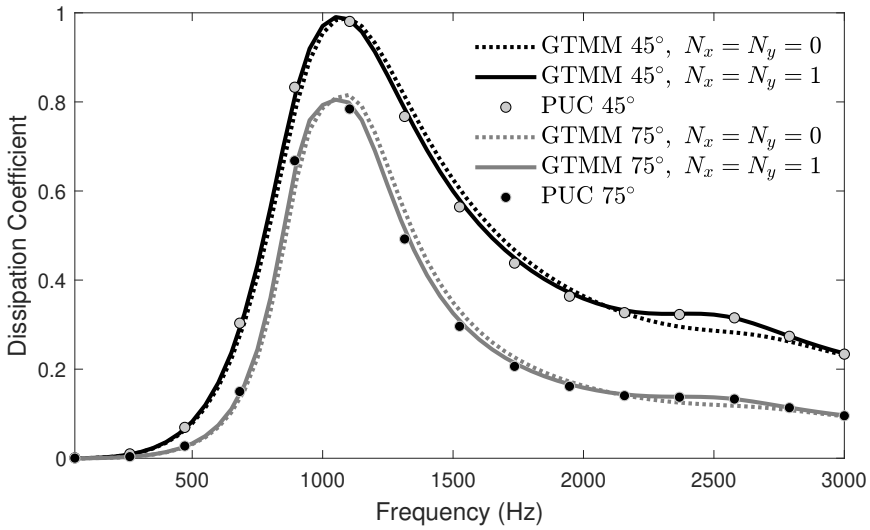

Figure 6: Dissipation coefficient at oblique incidences of a 19 mm thick rubber plate with spherical inclusions backed by a 15 mm thick steel plate.

The third case concerns a 40 mm thick polyurethane plate with infinite rectangular inclusions immersed in water on both sides. Inclusions are parallel to

the y-axis, have dimensions 15×20 mm^2, are 50 mm spaced along the x-axis and are filled with a soft polymer (modeled as a linear elastic solid). The materials properties are listed in Table 1. The fluid properties are $c_B = c_T = 1489$ ms^{-1} and $\rho_B = \rho_T = 1000$ kgm^{-3}. Figure 7a depicts the UC of the plate. The structure is modeled in three layers, the external 10 mm thick homogeneous layers and the intermediate 20 mm thick heterogeneous layer. The homogeneous layers are modeled with one Hexa8 element and $n_z = 20$. The heterogeneous layer is modeled with the Hexa18 mesh (quadratic along the x and z-axes and linear along the y-axis) depicted in Figure 7b and $n_z = 4$. Figure 8 compares the TL at normal incidence predicted by the proposed approach (GTMM) with the result produced by an alternative numerical approach (PUC) which uses a UC representing the whole plate. A perfect agreement is observed between the two methods over the whole frequency range in case of $(2 \times 8 + 1)$ Bloch modes along the x-axis ($N_x = 8$). Figure 9 shows the ratio between the smallest and largest eigenvalue of the matrix in Eq. (41) for different values of the maximum order of Bloch modes along the x-axis, N_x, ($N_y = 0$) and for two frequencies. It should be noted that for $N_x > 8$ the problem becomes ill conditioned, regardless of the frequency value, thus revealing that the adopted discretization is adequate to resolve the Bloch modes till $N_x = 8$.

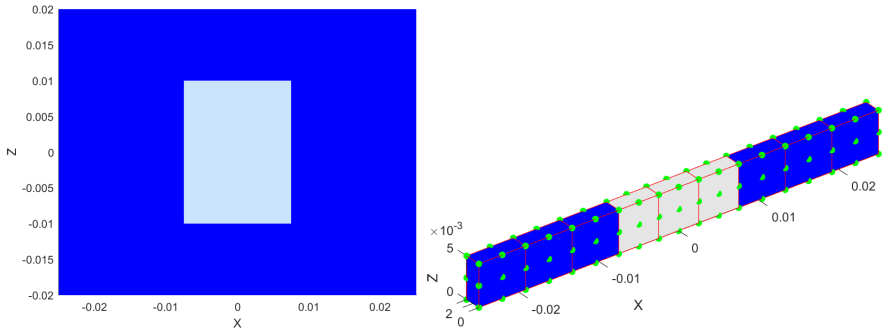

(a) Geometry of the global UC (b) Hexa18 mesh for the intermediate layer

Figure 7: UC of a 40 mm thick polyurethane plate with infinite rectangular inclusions.

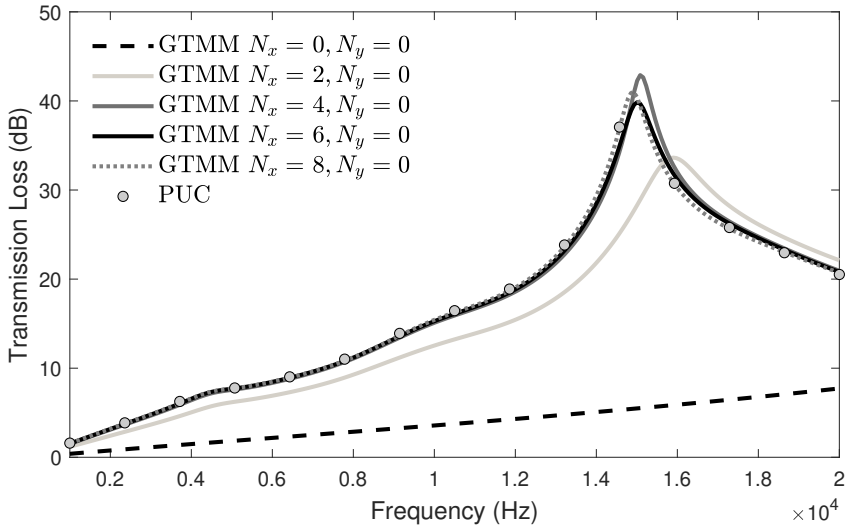

Figure 8: TL at normal incidence of a 40 mm thick polyurethane plate with infinite rectangular inclusions.

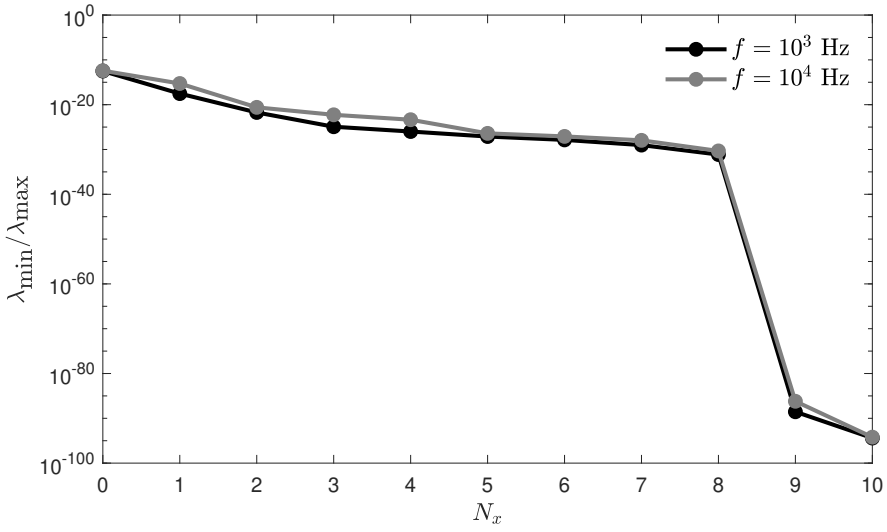

Figure 9: Inverse of the condition number of the matrix in Eq. (41) for a polyurethane plate with infinite rectangular inclusions ($N_y = 0$).

The last case concerns a doubly periodic Helmholtz resonator immersed in air on both sides. The resonator consists of a 25 mm long cylindrical neck with internal diameter of 30 mm located inside a 50 mm thick cylindrical chamber with internal diameter of 60 mm. The neck and the chamber are delimited by 2 mm thick rigid walls. Additional 2 mm thick air layers are locate on the top and on the bottom of the resonator. The resonators are 80 mm spaced along both the x-axis and the y-axis. The fluids properties are $c_B = c_T = 340$ ms^{-1} and $\rho_B = \rho_T = 1.284$ kgm^{-3}. A 0.1% of damping is applied to the air inside the resonator. The structure is modeled as a single layer. A quarter of the Tetra4 mesh of the layer UC is depicted in Figure 10. Figure 11 presents the TL at normal incidence of the resonator. It can be observed that Bloch modes are essential to capture the physics of the problem, in particular the resonance frequency value.

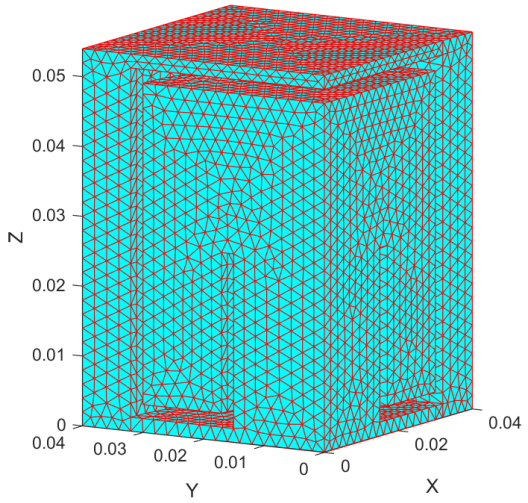

Figure 10: A quarter of the UC of a panel consisting of Helmholtz resonators.

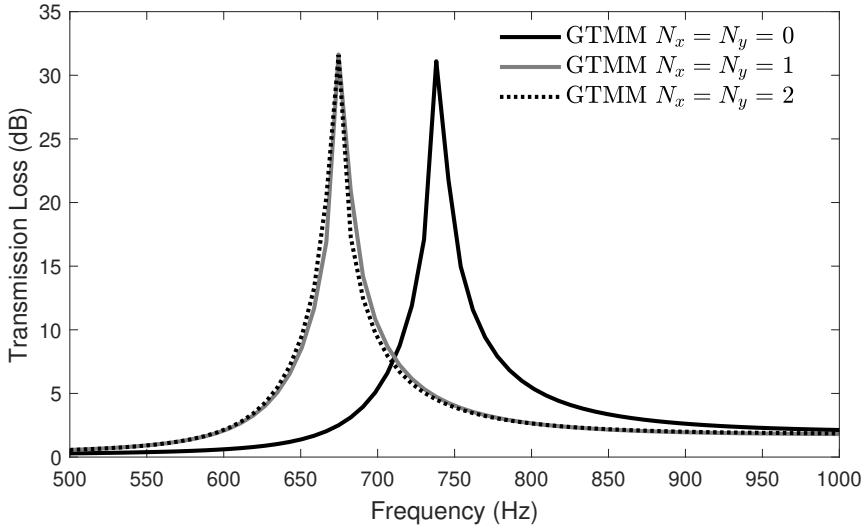

Figure 11: TL at normal incidence of a Helmholtz resonator with rigid walls.

	Density ρ (kgm^{-3})	Young's modulus E (MPa)	Poisson's ratio ν (-)	Damping μ (-)
Steel	7890	209000	0.275	0
Aluminum alloy	2690	74400	0.334	0
Host rubber	1100	29.7	0.498	0.30
Silicon rubber	1300	2	0.462	0.30
Polyurethane	1100	281	0.479	0.45
Polymer	12	0.8	0.1	0.30

Table 1: Properties of elastic materials.

4. Conclusions

An accurate and efficient generalized TMM for planar structures characterized by in-plane periodicity is proposed. The accuracy of the model in predicting acoustic indicators has been verified through agreement with alternative

approaches. It has also been proved that sound propagation may be strongly affected by Bloch modes, even in the low-frequency range, where the excitation wavelength is much larger than the periodic unit cells. The computational effort related to the proposed procedure depends on the adopted FE models and on the number of Bloch modes. However, in case of heterogeneous layers denoted by a through-thickness homogeneity, as in the third application discussed, a large number of Bloch modes allow to considerably reduce the number of dofs in the FE models, thus reducing the overall computational cost with respect to a solution achieved without Bloch modes. Moreover, homogeneous layers are modeled efficiently with a few finite elements by exploiting the ability to model only a portion of the thickness and by recovering the overall transfer matrix as power of the elementary one. Ultimately, the proposed approach could represent an effective acoustic tool for planar periodic non-homogeneous structures in a FE analysis environment, due to its versatility and efficiency. This will be in particular of value to the extensive work currently done by the vibro-acoustic community to develop metamaterials.

References

[1] L. Brillouin, Wave Propagation in Periodic Structures: Electric Filters and Crystal Lattices, Dover, 1946.

[2] D. Mead, A general theory of harmonic wave propagation in linear periodic systems with multiple coupling, Journal of Sound and Vibration 27 (2) (1973) 235 – 260. doi:http://dx.doi.org/10.1016/0022-460X(73)90064-3.

[3] A. L. Abrahamson, Flexural wave mechanics - An analytical approach to the vibration of periodic structures forced by convected pressure fields, Journal of Sound Vibration 28 (1973) 247–258. doi:10.1016/S0022-460X(73)80105-1.

[4] R. M. Orris, M. Petyt, A finite element study of harmonic wave propagation

in periodic structures, Journal of Sound and Vibration 33 (2) (1974) 223 – 236. doi:http://dx.doi.org/10.1016/S0022-460X(74)80108-2.

[5] R. M. Orris, M. Petyt, Random response of periodic structures by a finite element technique, Journal of Sound and Vibration 43 (1) (1975) 1 – 8. doi:http://dx.doi.org/10.1016/0022-460X(75)90199-6.

[6] J. Allard, N. Atalla, Propagation of sound in porous media : modelling sound absorbing materials 2nd edition, John Wiley & Sons, 2009.

[7] A. Parrinello, G. L. Ghiringhelli, Transfer matrix representation for periodic planar media, Journal of Sound and Vibration 371 (2016) 196–209. doi:10.1016/j.jsv.2016.02.005.

[8] D. L. Johnson, J. Koplik, R. Dashen, Theory of dynamic permeability and tortuosity in fluid-saturated porous media, Journal of Fluid Mechanics 176 (1987) 379–402. doi:10.1017/S0022112087000727.

[9] Y. Champoux, J. Allard, Dynamic tortuosity and bulk modulus in air-saturated porous media, Journal of Applied Physics 70 (4) (1991) 1975–1979. doi:10.1063/1.349482.

[10] N. Atalla, R. Panneton, P. Debergue, A mixed displacement-pressure formulation for poroelastic materials, The Journal of the Acoustical Society of America 104 (3) (1998) 1444–1452. doi:10.1121/1.424355.

[11] J.-P. Groby, O. Dazel, A. Duclos, L. Boeckx, L. Kelders, Enhancing the absorption coefficient of a backed rigid frame porous layer by embedding circular periodic inclusions, The Journal of the Acoustical Society of America 130 (6) (2011) 3771–3780. doi:10.1121/1.3652865.

[12] F. Sgard, N. Atalla, R. Panneton, Finite element modelling of the acoustic properties of rubber containing inclusions, Tech. Rep. RDDC-2014-C235, Mecanum Inc Sherbrooke, QC Canada (2014).